

Structure and dynamics of turbulent boundary layer flow over healthy and algae-covered corals

Jonathan B. Stocking¹ · John P. Rippe² · Matthew A. Reidenbach²

Received: 27 October 2015 / Accepted: 2 April 2016 / Published online: 9 April 2016
© Springer-Verlag Berlin Heidelberg 2016

Abstract Fine-scale velocity measurements over healthy and algae-covered corals were collected in situ to characterize combined wave-current boundary layer flow and the effects of algal canopies on turbulence hydrodynamics. Data were collected using acoustic Doppler velocimetry and particle image velocimetry. Flow over healthy corals is well described by traditional wall-bounded shear layers, distinguished by a logarithmic velocity profile, a local balance of turbulence production and dissipation, and high levels of bed shear stress. Healthy corals exhibit significant spatial heterogeneity in boundary layer flow structure resulting from variations in large-scale coral topography. By contrast, the turbulence structure of algae-covered corals is best represented by a plane mixing layer, with a sharp inflection point in mean velocity at the canopy top, a large imbalance of turbulence production and dissipation, and strongly damped flow and shear stresses within the canopy. The presence of an algal canopy increases turbulent kinetic energy within the roughness sublayer by ~ 2.5 times compared to healthy corals while simultaneously reducing bed shear stress by nearly an order of magnitude. Reduced bed shear at the coral surface and within-canopy

turbulent stresses imply reduced mass transfer of necessary metabolites (e.g., oxygen, nutrients), leading to negative impacts on coral health.

Keywords Corals · Turf algae · Turbulence · Wave-current flow · Canopy flow

Introduction

As sessile, benthic organisms, corals depend on mass transfer to and from the overlying water column for many biologically necessary processes, including photosynthesis by endosymbiotic zooxanthellae, carbonate skeleton building, larval dispersal and settlement, and nutrient and dissolved gas exchange (Atkinson and Bilger 1992; Dennison and Barnes 1988). The mass transfer required for these processes can be achieved through diffusion alone, but even small amounts of fluid advection can greatly enhance the efficiency of mass flux (Mass et al. 2010). Corals are typically found in shallow, oligotrophic tropical and subtropical coastal oceans in which fluid motion generated by both currents and waves supplies the momentum required for mass-exchange processes. The dominant factor controlling the vertical transport of mass between the water column and coral surface is the fine-scale hydrodynamics of the turbulent bottom boundary layer (BBL) adjacent to the coral surface (Reidenbach et al. 2007).

Within coral reef communities, many other organisms directly compete with corals for resources in the nutrient-poor marine habitat, and as a result, can alter BBL dynamics. In particular, benthic macroalgae often exhibit a competitive advantage for space and light under conditions of limited herbivory or excessive nutrient loading (Jompa and McCook 2002). Algal turfs impact boundary layer

Communicated by Biology Editor Dr. Mark R. Patterson

Electronic supplementary material The online version of this article (doi:10.1007/s00338-016-1446-8) contains supplementary material, which is available to authorized users.

✉ Jonathan B. Stocking
jbs4yq@virginia.edu

¹ Department of Mechanical and Aerospace Engineering, University of Virginia, 122 Engineer's Way, PO Box 400746, Charlottesville, VA 22904, USA

² Department of Environmental Sciences, University of Virginia, Charlottesville, VA, USA

hydrodynamics by altering the mean velocity profile (Carpenter and Williams 1993), in addition to direct interactions such as overgrowth and shading, chemical attack, and surface abrasion (McCook et al. 2001). Little is known, however, about how algae affect the turbulence regime within the BBL, which has important implications for vertical transport and mixing between the coral and overlying water column, critical processes for coral mass transfer, but broadly applicable to other substrates with algal canopies as well.

Hydrodynamics of the turbulent boundary layer

Along the surface of an individual coral, the overlying water column interacts through friction with the fixed coral boundary, producing a layer of shear flow that generates a turbulent wall boundary layer (Reidenbach et al. 2006b). The BBL is composed of: (1) an inner layer very near the wall, in which fluid viscosity is the controlling scale and which typically extends a few hundred microns in elevation; and (2) an outer layer in which the flow resembles inviscid, wall-free turbulence and whose vertical range depends on the scale of the maximum size of turbulent eddies (Kundu and Cohen 2008). Connecting these two regions is an overlap layer, called the inertial sublayer, which typically measures 15–20% of the total BBL thickness and where inertial effects dominate, causing the velocity to follow a logarithmic profile, a key characteristic of wall-bounded shear flow.

Close to the coral–water interface within the inner layer, fluid viscosity dampens turbulent motions, and molecular diffusion is the primary mechanism of vertical transport. The production or consumption of dissolved materials by the coral surface creates a concentration gradient, forming a diffusive boundary layer (DBL). Typically less than 1.0 mm thick, the size of the DBL is controlled by surface roughness, flow speed, and the molecular diffusivities of relevant dissolved materials (e.g., O_2 , CO_2 , PO_4^{3-} , NH_4^+). Ultimately, the DBL governs the rate of mass flux to and from individual coral polyps and acts as a bottleneck for mass transfer (Jørgensen and Des Marais 1990). Increases in wall shear stress τ_{wall} and in turbulent kinetic energy q^2 reduce the thickness of the DBL and can enhance mass flux across this water–substrate interface (Hondzo 1998; Røy et al. 2002). Further, corals themselves may actively disrupt the DBL by employing ciliary beating to generate microscale vortical flows that enhance mass transfer up to fourfold compared to molecular diffusion alone (Shapiro et al. 2014).

Above the DBL, vertical mass transport is primarily controlled by turbulent diffusivity v_r , the magnitude of which is proportional to the ratio of turbulent kinetic

energy q^2 to the turbulent dissipation rate ε , i.e., $v_r \propto (q^2)^2/\varepsilon$ (Kundu and Cohen 2008). Higher levels of turbulent kinetic energy (TKE), therefore, act to mix and transport both dissolved and particulate matter above the coral surface more efficiently. Additionally, increases in turbulence intensity—defined as the ratio of turbulent fluctuations to the mean free-stream velocity—have been shown to enhance mass transfer rates (Falter et al. 2007). Of interest for this study are the biological implications for coral health due to the turbulent boundary layer, and thus, turbulent control on diffusive and convective mass transport processes.

Boundary layer alterations due to waves and canopies

Coral reef ecosystems are generally exposed to a combination of tide-driven unidirectional currents and wave-driven oscillatory motion (Monismith 2007). Combined wave-current flows feature a non-linear interaction between the steady turbulent boundary layer created by the unidirectional current and the thin, time-varying wave boundary layer created by the oscillatory flow (Grant and Madsen 1979). The time-averaged velocity profile for combined wave-current flow has been shown to be logarithmic within and above the wave boundary layer, though with different slopes for each region (Fredsoe 1984). The presence of waves significantly impacts reef biophysical processes, e.g., enhancing vertical flow rates and mass flux within branching corals (Reidenbach et al. 2006a).

Additionally, the presence of a surface canopy can significantly alter boundary layer hydrodynamics, evident by a sharp inflection in velocity at the canopy top, which results in increased levels of shear just above the canopy (Raupach et al. 1996). For unidirectional flow, turbulent stresses within the canopy quickly dampen as the canopy floor is approached (Finnigan 2000). Under oscillatory forcing, canopy structure is important, such that rigid canopies generate larger turbulent stresses in the upper canopy compared to above the canopy (Reidenbach et al. 2007), whereas flexible canopies dampen turbulent stresses and vertical transport within the canopy compared to above it (Ghisalberti and Nepf 2006).

Investigations into algal canopy flows have measured mean flow quantities, finding that higher canopies extend the vertical range of the overlying momentum boundary layer compared to lower canopies (Carpenter and Williams 1993). Unidirectional flow speed has also been shown to control vertical profiles of oxygen concentration over algae-covered corals, with higher flow rates reducing the DBL thickness (Brown and Carpenter 2013), thereby demonstrating a key role for algal canopies in controlling

coral mass flux. More broadly, reef algal turfs make important contributions in their own right to benthic primary production, which sustains higher trophic levels in reef food webs. Understanding the turbulent hydrodynamics of algal canopy flow has wide applicability; however, detailed measurements of turbulence characteristics over algae-covered corals have not been made, and little is known about how algal turfs may modify the structure and type of boundary layer turbulence, especially for combined wave-current flow environments.

The purpose of this study is to provide a detailed in situ characterization of the fine-scale turbulent boundary layer dynamics of both healthy and degraded, algae-covered coral exposed to naturally occurring wave-current flows. This study seeks to answer the following questions:

1. What are the hydrodynamic characteristics—specifically mean velocity, bed shear stress, Reynolds stress, TKE, and turbulent production and dissipation—that describe the boundary layer at a coral–water interface under combined wave-current conditions?
2. How does an algal turf canopy alter the structure and dynamics of the turbulent boundary layer, and what are the implications for mass transfer at the coral–water interface?

Using a combination of an in situ particle image velocimetry (PIV) system and a profiling acoustic Doppler velocimeter (ADV), boundary layer flow profiles were recorded over the scleractinian coral *Siderastrea siderea* in the coastal Caribbean waters of Bocas del Toro, Panamá.

Methods

Study site

Experiments were conducted on the fringing coral reef in the Caribbean archipelago of Bocas del Toro, Panamá (9°21'N, 82°16'W). The study site (Fig. 1) is situated near

the Smithsonian Tropical Research Institute approximately 50 m off the bayside shore of Isla Colón. The reef begins just below the mean low tide mark and extends to depths >20 m. The reef composition is dominated by the branching coral *Porites furcata* and the lobate (brain) corals *Colpophyllia natans* and *S. siderea*, with a variety of sponges, anemones, and urchins also common. Measurements were collected over healthy and algae-covered *S. siderea* corals (Fig. 2a, b) situated at depths of approximately 1.0–2.5 m during two site visits: 7–20 June 2012 and 12–30 July 2013. The site is exposed to mixed semidiurnal tides with a tidal range of approximately 0.5 m (Li and Reidenbach 2014). The wave environment is primarily wind-driven from the southeast, with mean winds of 1.9 m s^{-1} during June 2012 and 1.8 m s^{-1} during July 2013.

Coral and algal morphology

The boulder-shaped species *S. siderea* was selected because of its prevalence at the study site, uniform surface topography, and susceptibility to algal overgrowth. Polyps of sampled corals measured approximately 0.25 cm in height, creating a slightly dimpled surface at the coral–water interface. All measurements were collected during the day when polyp tentacles were retracted so that a relatively uniform roughness height could be estimated. Measurements were taken as close as possible to the center of the corals to reduce the effects of large-scale topographic features that might generate leading or trailing edge effects, and efforts were made to minimize the influence of non-local turbulence from surrounding structures by selecting spatially isolated corals and aligning the instrument frame with the dominant flow direction (Fig. 3). The influence of non-local turbulence, however, has been shown to be relatively limited, enhancing mass transfer coefficients up to only $\pm 10\%$ for very high levels of free-stream turbulence (Falter et al. 2007).

Fig. 1 Site map of island archipelago of Bocas del Toro, Panamá. The study site is located on landward side of Isla Colón

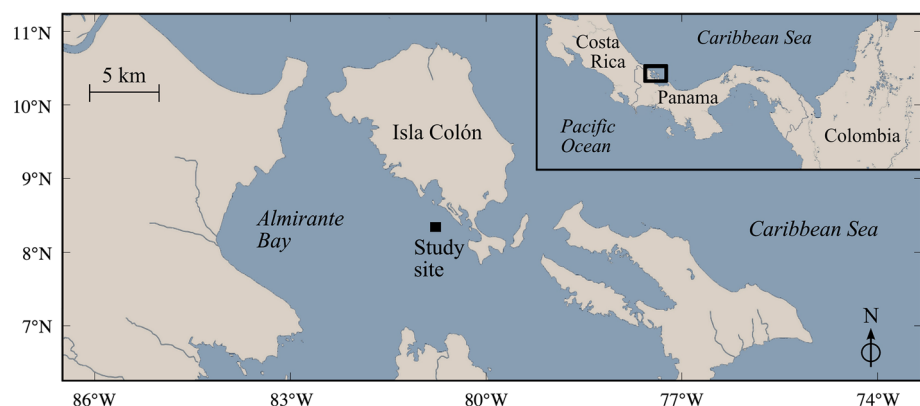


Fig. 2 **a** Vectrino acoustic Doppler velocimeter probe tip positioned above a healthy *Siderastrea siderea* coral. **b** Probe tip positioned above algae-covered *S. siderea* coral. Note white patch of bleached coral exposed after algae removal for in-canopy flow measurements

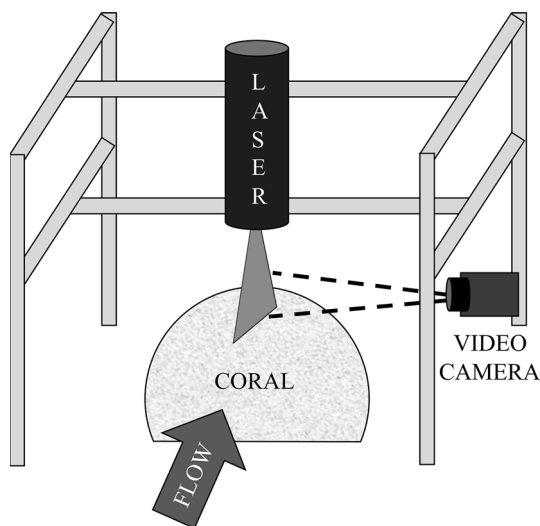
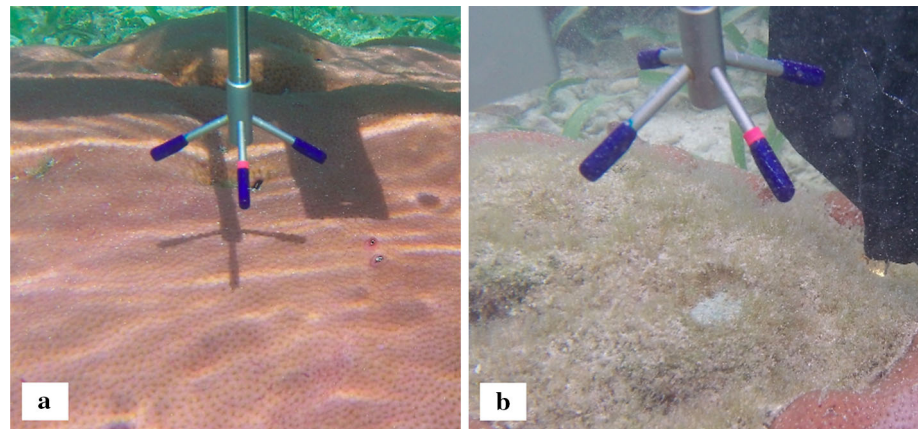


Fig. 3 Schematic of instrument frame with particle image velocimetry experimental setup over healthy *Siderastrea siderea* coral. The frame was aligned with dominant flow direction to avoid non-local turbulence from frame legs. Acoustic doppler velocimeter (ADV) measurements were obtained using the same frame setup with the ADV instrument replacing the laser

Siderastrea siderea corals with algal turfs that colonized the surface in discrete patches were selected in close proximity to the healthy corals. Polyps beneath the canopy were degraded, but likely still in a recoverable state. The algae found in the Bocas del Toro reef, common among Caribbean marine habitats, is a multispecies assemblage of green, red, and brown seaweeds with filamentous cyanobacteria (Fricke et al. 2011). Estimates of algal canopy density λ were made based on the total algal frontal area per unit ground area (Raupach et al. 1996), given as $\lambda \equiv \frac{hd}{A/n}$, where h is the canopy height, d is the algal stem diameter, A is the ground area, and n is the number of stems in the measured area. Typical values for canopy parameters were estimated as $h \approx 10$ mm, $d \approx 0.2$ mm, $A \approx 100$ mm², and $n \approx 20$, which yields a canopy

roughness density of $\lambda \approx 0.4$, significantly higher than the threshold of $\lambda > 0.1$ that defines a “dense” vegetation canopy (Nepf 2012).

Instrumentation

Three-component velocity measurements (horizontal u , lateral v , and vertical w) were collected using a profiling acoustic Doppler velocimeter (Vectrino Profiler, Nortek AS) at a sampling rate of 25 Hz for burst intervals ranging between 5 and 10 min (7500–15,000 samples per burst). The minimum burst length was set to allow for a balance between obtaining convergence of mean velocity and turbulent quantities while still maintaining stationarity within changing wave and tidal conditions (Gross and Nowell 1983). Burst intervals were rotated into the dominant streamwise direction u during post-processing. Stationarity of the tidal current for each burst was verified using the nonparametric reverse arrangements test ($N = 10, \alpha = 0.05$; Bendat and Piersol 2010), and bursts exhibiting non-stationarity were omitted. Figure 4 plots the full instantaneous velocity record for a sample 10-min burst and illustrates the stationarity of the background current. The instrument was mounted to an aluminum frame with a width and length of 1 m and height-adjustable legs used to minimize instrument tilt. Velocity profiles approximately 3 cm high with a resolution of 1 mm were obtained over the coral surface (Fig. 2a). For the algae-covered corals, a small patch (~ 1 cm²) of algae directly beneath the probe tip was cleared to allow for within-canopy measurements (Fig. 2b). To accommodate the double-averaging technique typically used to describe canopy flows (Nikora et al. 2007), multiple spatial measurements of time-averaged profiles were collected over the same and different corals. Though simultaneous spatial measurements were not possible due to the limited space in the canopy patch, normalization of multiple spatial profiles

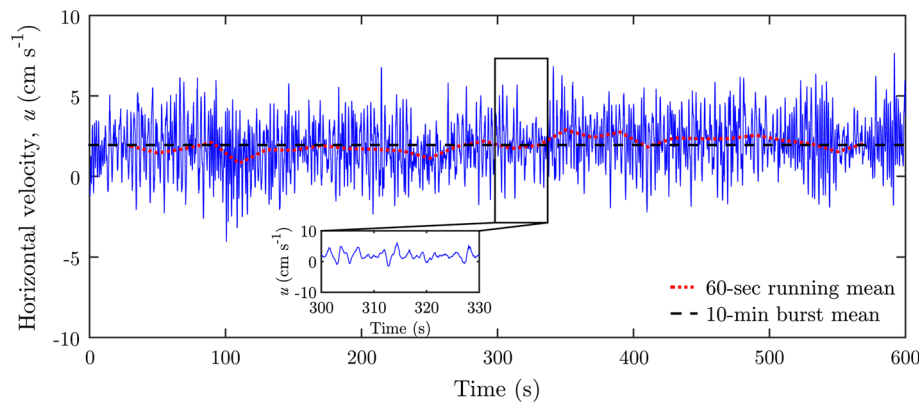


Fig. 4 Typical record of instantaneous horizontal velocity u for a 10-min burst. *Black dashed* line shows background mean, i.e., tidal current velocity, over entire record. *Red dotted* line plots 60-s running mean and shows consistent stationarity about the burst mean,

confirmed quantitatively using reverse arrangements test. *Inset* plot expands a 30 s segment of the burst to illustrate the spectral wave signal with dominant period of 2.7 s. Data taken from a single ADV measurement bin ~ 1.5 cm above healthy coral surface

by the free-stream velocity (described below) allowed for a single double-averaged profile to be computed.

As an instrument class, ADVs have known difficulties measuring near boundaries due to interference of the reflected acoustic pulses echoing from solid boundaries (Voulgaris and Trowbridge 1998). The height above the boundary for which echoes bias velocity estimates can be identified by a sharp increase in the signal-to-noise ratio (SNR) and depends on boundary material and flow conditions (Rusello 2012). We measured this contamination height for each burst by identifying the transition from decreasing to increasing SNR derived from the mean of the four transducer heads. The location of the coral surface was determined by the instrument's bottom detection measurement and confirmed by steady zero velocity components. Together, these two locations determined the height of echo interference, which extended ~ 3 mm above the coral surface and is indicated by a gray box in all plots of ADV data.

A second set of independent velocity measurements used to obtain spatial information of velocity structure along the coral surface was made using a custom-fabricated underwater PIV system. A 532-nm green laser (300 mW Hercules Series, Laserglow Technologies) was secured inside a watertight housing and directed through a convex lens at the housing base to create a continuous, two-dimensional sheet of laser light. The laser housing was mounted on the instrument frame above the coral and aligned with the dominant flow direction. Perpendicular to the laser sheet, an underwater video camera (Sony HDR-CX160, Sony Electronics Inc.) was attached to the frame and fitted with a 530 ± 3 nm bandpass filter (Andover Corporation) to remove excess daylight (Fig. 3). The camera recorded a field-of-view of approximately 5×6 cm at 30 frames s^{-1} . Free-floating particulates in the

water column served as velocity tracers and were illuminated and recorded as they passed through the laser sheet plane. PIV measurements were only performed over the healthy coral since the algal canopy blocked the field-of-view of the camera. Raw PIV video records were processed using open-source MatPIV 1.6.1 software written for MATLAB (Sveen 2004), which implements a hybrid digital PIV technique using iterative windowing to a final interrogation resolution of 32×32 pixels. Outliers were identified using global mean and local median filters (± 3 and ± 2.5 standard deviations, respectively) and replaced via linear interpolation. Accuracy of PIV measurements was previously determined in a tow-tank to be $\pm 6\%$ of the mean velocity magnitude (Reidenbach et al. 2008).

Analysis of turbulence statistics

In combined wave-current flow, wave orbital motions outside the thin wave boundary layer are irrotational and do not contribute to the shear-generated turbulence from the current. However, wave orbitals induce large variances in the horizontal and vertical velocity components, which mask velocity variances due to turbulence, making it necessary to separate the wave and turbulence parts of the signal. For wave-current flows, the components of the total instantaneous velocity u can be separated via Reynolds decomposition according to:

$$u = \bar{u} + \tilde{u} + u' \quad (1)$$

where \bar{u} is the mean current velocity, \tilde{u} is the instantaneous wave orbital velocity, and u' is the instantaneous turbulent velocity. Wave and turbulence perturbations were separated using a spectral decomposition technique called the phase method (Bricker and Monismith 2007), which converts the temporal velocity record into frequency space via

Fourier transformation and isolates the wave stress (evident as the clear wave peak in the sample power spectrum of Fig. 5) using the phase lag between horizontal and vertical components of the two-sided cross-spectral density. Details of the phase method can be found in Electronic Supplementary Material (ESM) S1 and in Bricker and Monismith (2007).

Following separation of the burst-averaged wave and turbulence signals, turbulent stresses were used to estimate the components of the TKE budget, given in tensor notation as:

$$\frac{\partial \overline{q^2}}{\partial t} + \overline{u_j} \frac{\partial \overline{q^2}}{\partial x_j} = - \underbrace{\overline{u'_i u'_j} \frac{\partial \overline{u_i}}{\partial x_j}}_{P_S} - \underbrace{\overline{u'_i u'_j} \frac{\partial \overline{u''_i}}{\partial x_j}}_{P_W} - \underbrace{\frac{\partial \overline{q^2 u'_j}}{\partial x_j}}_{T_i} - \underbrace{\frac{\partial \overline{p' u'_j}}{\partial x_j}}_{T_p} - \varepsilon \tag{2}$$

where $q^2 = 0.5(\overline{u'u'} + \overline{v'v'} + \overline{w'w'})$ is TKE, P_S is turbulence shear production, P_W is turbulence wake production (where the double primes signify deviations from a spatial average), T_i is advective turbulent transport, and T_p is pressure-driven transport (Finnigan 2000). Equation (2) omits buoyancy production, as well as dispersive and viscous turbulent transport terms, which are all assumed to be negligible. The left-hand side of Eq. (2) represents the temporal change and spatial advection of TKE, respectively and is equal to zero for a stationary, fully developed shear layer. The degree of development is described by the wave Reynolds number $Re_o = (\tilde{u}_{om} A_{max})/\nu$, where \tilde{u}_{om} is the maximum near-bed wave orbital velocity, A_{max} is the near-bed wave orbital amplitude, and ν is fluid viscosity. The dominant terms on the right-hand side of Eq. (2) are production and dissipation ε , which are measured directly, and the transport terms are set equal to the difference

between production and dissipation. Wake production, which results from vortex shedding from individual canopy elements, is only relevant for algae-covered corals. Turbulent dissipation rates ε were calculated using the inertial subrange dissipation method (IDM), described in ESM S2.

Bed shear stress τ_{bed} was calculated using the formulation of Wiberg and Smith (1983), defined as:

$$\tau_{bed} = \sqrt{\tau_c^2 + \tau_w^2} \tag{3}$$

where τ_c is bed shear due only to currents and τ_w is bed shear due only to wave orbital motions. The current-induced bed shear stress is estimated using near-bed TKE outside the wave boundary layer, according to Soulsby and Dyer (1981):

$$\tau_c = 0.19 \rho q^2 \tag{4}$$

The wave-induced contribution is parameterized using the near-bottom wave orbital velocity \tilde{u}_{om} and a wave friction factor f_w (Jonsson 1966):

$$\tau_w = 0.5 f_w \rho \tilde{u}_{om} \tag{5}$$

The appropriate wave friction factor is determined by the ratio of the wave amplitude a , i.e., half of the wave height, to the bed roughness k_s , and for the corals studied, is given by $f_w = 0.4(alk_s)^{-3/4}$ (Madsen et al. 1988).

Results

A total of eight ADV records over healthy corals and four ADV records over algae-covered corals met the inclusion criteria for data analysis. Table 1 lists key wave and current parameters, including wave Reynolds numbers, for healthy and algae-covered corals. As conditions varied across records, we chose to normalize velocities and turbulence statistics using the root-mean-squared (rms) velocity, which measures total fluid motion from waves and currents, and is given by:

$$u_{rms} = \sqrt{\overline{u^2}} \tag{6}$$

where the overbar represents time-averaging of the squared instantaneous horizontal velocity u for an individual record. The horizontal free-stream rms velocity $u_{\infty,rms}$ was calculated for each burst by averaging the ten measurement bins farthest from the coral surface, which varied by less than 3%, indicating a steady, ‘local’ free-stream velocity.

Velocity structure and Reynolds stresses

Figure 6a shows vertical profiles of rms horizontal velocity for healthy coral (in red) and algae-covered coral (in green). Profiles plot the normalized mean \pm one standard

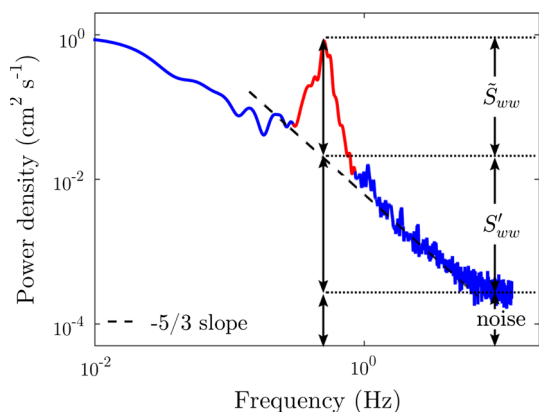


Fig. 5 Representative power spectral density (PSD) plot of turbulent vertical fluctuations obtained by ADV for a single measurement bin ~ 1.5 cm above the healthy coral. The wave peak \tilde{S}_{ww} , highlighted in red and bound by a $-5/3$ fit to the inertial subrange, is subtracted from the total power density (minus noise) to give the turbulent power density S'_{ww}

Table 1 Flow conditions for healthy (H) and algae-covered (A) corals

Coral case	Root-mean-square horizontal velocity $u_{\infty,rms}$ (cm s ⁻¹)	Mean current velocity $\bar{u}_{\infty,c}$ (cm s ⁻¹)	Maximum wave orbital velocity \tilde{u}_{om} (cm s ⁻¹)	Mean wave period T (s)	Mean wave height H (cm)	Wave Reynolds number Re_o
H1	1.41	0.48	3.91	2.00	7.73	548.1
H2	1.90	0.68	4.93	2.01	9.64	873.9
H3	1.96	1.57	3.04	3.72	2.02	613.8
H4	2.34	0.83	9.66	2.21	15.62	3695.6
H5	2.35	0.28	4.80	2.28	7.42	937.9
H6	2.41	1.91	4.63	2.69	3.37	1030.5
H7	2.54	0.37	4.99	2.10	8.87	935.0
H8	4.26	0.86	13.83	2.41	19.69	8229.8
A1	0.89	0.30	2.30	1.68	1.99	157.9
A2	1.08	0.41	2.78	1.27	3.87	174.7
A3	1.29	0.26	2.14	1.38	2.46	112.8
A4	1.40	0.42	2.93	1.52	2.88	232.4

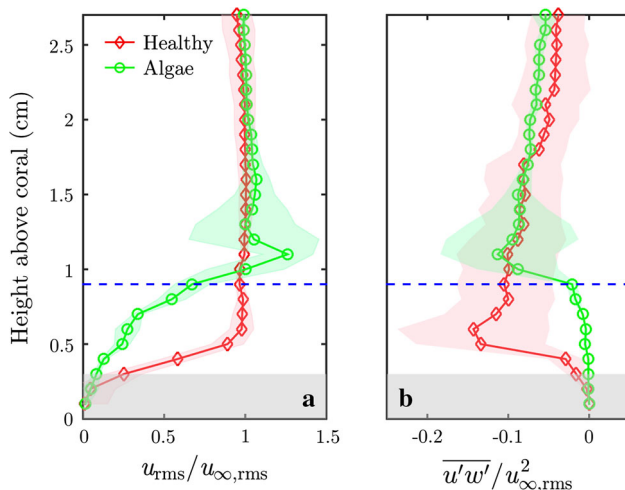


Fig. 6 **a** Vertical profiles of root-mean-square (rms) horizontal velocity normalized by free-stream rms velocity. *Markers* indicate heights of measurement bins for ADV, and *shaded* regions represent \pm one standard deviation from mean. *Horizontal blue dashed* line indicates approximate height of canopy for algae-covered coral, and *gray* area represents region of “acoustic reflection” bias, in which data points are less reliable. **b** Vertical profiles of turbulent Reynolds stress normalized by square of the rms free-stream velocity

deviation of all included bursts ($n = 8$ for healthy corals, $n = 4$ for algae-covered corals). RMS horizontal velocities over the healthy corals show a steep increase from the “no-slip” boundary condition at the coral surface and reach the 99% free-stream rms velocity threshold approximately 5 mm above the coral. For bursts in which rms wave orbital velocities are much larger than mean current velocities, the thicker current-only boundary layer can be “masked” by the wave velocities in the total rms velocity profile (evident

in the log profile below). To determine the degree to which the measured turbulent boundary layer over the healthy corals approximates a theoretical log-law regime, we isolated the mean current profile from a typical ADV burst and compared it to the predicted profile both within the wave boundary layer (WBL) and within the superimposed current boundary layer. For flows over rough surfaces, the profile of the current is predicted to be logarithmic, with differing slopes for each region, according to:

$$\bar{u}_c = \frac{\beta}{\kappa} \ln \frac{30z}{\gamma} \tag{7}$$

where $\beta = \frac{u_{*c}^2}{u_{*cw}}$ and $\gamma = k_s$ within the WBL and $\beta = u_{*c}$ and $\gamma = k_{sa}$ above the WBL (Grant and Madsen 1979). u_{*c} and u_{*cw} are friction velocities due to steady flow only and combined wave-current flow, respectively. k_s is bottom roughness, set equal to the coral polyp size (~ 0.25 cm), and k_{sa} is the “apparent” bottom roughness, which includes the actual bottom roughness and an additional roughness component resulting from the drag generated by the WBL and felt by the current boundary layer. The value of k_{sa} is found by matching the mean velocity at the end of the WBL to the mean velocity at the start of the current boundary layer.

Figure 7 shows record H1 as a representative dataset comparing the profile of the mean current velocity to the theoretical log-law inertial subrange. Excellent agreement between the two profiles exists between approximately $z = 3$ and $z = 9$ mm. The transition from WBL to current boundary layer—indicated by the increase in slope of the predicted mean velocity profile and marked by the vertical arrow—occurs approximately 5 mm above the coral, matching the thickness estimated from the rms profile.

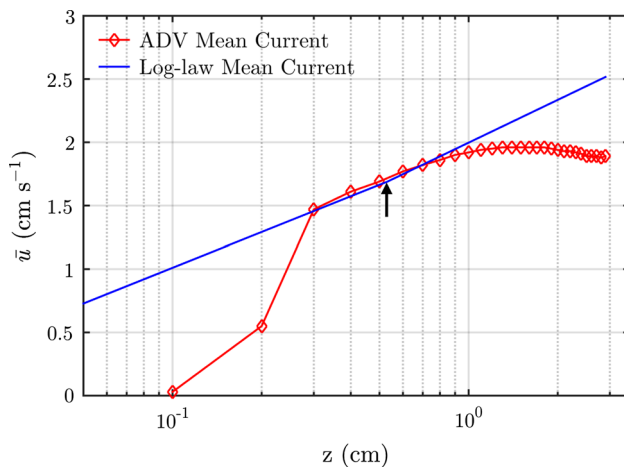


Fig. 7 Comparison of a theoretical combined wave-current logarithmic profile for mean velocity for an inertial boundary layer (in blue) versus measured mean velocity profile over healthy coral (in red). The arrow indicates the transition from wave to current boundary layer, i.e., where the slope of the logarithmic line increases

In contrast to the healthy coral, the profile of rms horizontal velocity over the algae-covered coral (Fig. 6a) is characterized by a distinct inflection point just above the canopy top and a strong shear layer due to the frictional drag imparted on the flow by the algae. Within the canopy, horizontal velocities decay rapidly and exhibit an almost linear profile near the coral surface. Compared to the healthy coral, the algae-covered corals possess reduced velocities near the coral surface, where for example, the 50% free-stream velocity threshold is reached 8 mm above the coral surface compared to only 3 mm above the healthy coral.

Normalized Reynolds stress profiles over the healthy coral (Fig. 6b) show a peak approximately 5 mm above the surface, indicating maximum rates of turbulent mixing very near coral polyps. Above this region, Reynolds stresses remain fairly steady between $z = 6$ and $z = 9$ mm—above the WBL but still within the current boundary layer—suggesting the presence of a constant stress layer typical of equilibrium boundary layer flows. Higher in the water column, turbulent stresses trend toward zero, though $\overline{u'w'}$ remains non-zero likely due to transported non-local turbulence. The normalized Reynolds stress profile for the algae-covered coral peaks just above the canopy top, where the inflection in velocity occurs. Above this, no constant stress layer is evident; rather, the stresses decrease linearly toward zero. Direct comparison of the profiles shows that Reynolds stresses for the healthy coral do not approach zero until nearly the surface of the coral, whereas the algal canopy dampens Reynolds stresses to close to zero at approximately 8 mm above the coral–water interface.

Turbulent kinetic energy budget

For the healthy coral, vertical profiles of normalized mean TKE (Fig. 8a) show a rapid rise in the near-bed region, peaking ~ 5 mm above the bed, and remaining constant throughout the upper profile. The algae-covered corals, by contrast, exhibited nearly three times higher levels of TKE above the canopy compared to the healthy corals, owing to the interaction between the flow and the drag generated by the canopy top. Normalized TKE levels for healthy corals demonstrate low variance across wave and tidal conditions, whereas the algal profile features higher variability, likely due to the inhomogeneity of algal turfs. Within the canopy, TKE levels are drastically reduced and fall below healthy coral levels for regions below $z = 6$ mm.

Turbulence production over the healthy corals, shown in Fig. 8b, exhibits a sharp peak approximately 5 mm above the coral surface due to the steep velocity gradients and peak Reynolds stresses at this elevation. Above this height, production decreases rapidly and is effectively zero for elevations greater than $z = 6$ mm. Similarly, turbulence dissipation over the healthy corals (Fig. 8c) peaks at $z = 5$ mm above the coral surface and is similar in magnitude to production, indicating a local equilibrium balance. The decrease in dissipation rate with height is gradual and remains slightly non-zero throughout the water column, which suggests dissipation of non-local turbulence may be occurring.

Algae-covered corals exhibit two strong peaks in turbulence production above the canopy (Fig. 8b), one positive and one negative, and another moderate production region within the upper canopy, a result of fine-scale wake shedding. The peaks above the canopy result from the velocity shear layer, and the inflection in the velocity profile generates the negative gradients responsible for “negative” production. Higher in the water column, production falls to zero, similar to the healthy corals. The profile of turbulence dissipation over the algae-covered corals (Fig. 8c) shows a peak in ε , with large variability, at an elevation higher than the two shear production peaks, indicating non-local equilibrium and significant turbulent transport in this region.

Bed shear stress

For the healthy corals, near-bed values of q'^2 , \tilde{u}_{om} , and $\overline{u'w'}$ required to estimate bed shear stress were selected based on their peak values within the boundary layer. However, the algal canopy dampens vertical transport so that peak values of mean and turbulent quantities above the canopy are not appropriate predictors of stresses at the coral surface. For dense canopies, the penetration depth h_p of momentum,

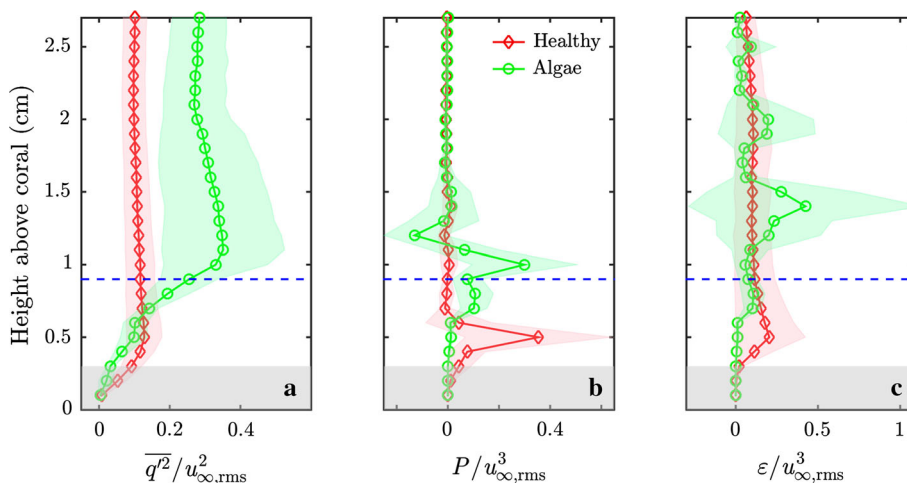


Fig. 8 Vertical profiles of **a** turbulent kinetic energy **b** turbulent production, and **c** turbulent dissipation rate, normalized by square and cube of the root-mean-square freestream velocity, respectively. *Markers* indicate heights of measurement bins for ADV, and *shaded*

regions represent \pm one standard deviation from mean. *Horizontal blue dashed* line indicates approximate height of canopy for algae-covered coral, and *gray area* represents region of “acoustic reflection” bias, in which data points are less reliable

called the “vertical exchange zone”, has been shown to extend to approximately $z/h_c \approx 0.7$, where h_c is canopy height (Finnigan 2000). Below this height, turbulent terms remain relatively constant, so values just below h_p were used to calculate bed shear stress. These estimates were compared to direct estimates of bed shear stress using total Reynolds stresses $\overline{u'w'}$, which include contributions from both current and wave motion, according to the relationship $\tau_{bed} = -\rho\overline{u'w'}$. Figure 9 compares normalized bed shear stress calculated using each technique for healthy and algae-covered corals. Results show that the mean bed shear stress for healthy corals was nearly an order of magnitude greater than for the algae-covered corals (Welch’s t test, $t = 4.1$, $df = 7$, $p < 0.01$).

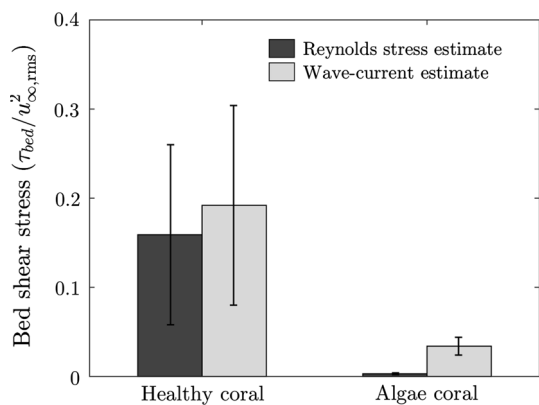


Fig. 9 Comparison of normalized bed shear stress for healthy and algae-covered corals using two independent techniques and showing statistically significant difference in means between healthy and algae-covered corals (Welch’s t test, $t = 4.1$, $df = 7$, $p < 0.01$). *Error bars* represent \pm one standard deviation from mean

PIV spatial analysis of mean and turbulent flow structure

Figure 10a shows the rms velocity field for PIV data consisting of 900 image pairs, totaling 30 s. The mean of rms velocities for the top 1 cm is 0.85 cm s^{-1} , and the vertical profiles show a trend similar to the ADV measurements with a sharp decrease near the surface. A key difference, however, is the spatial variability of the velocity around the coral surface. The leading edge of the coral structure (left side of image) causes a much smaller decrease in near-surface velocities compared to the flatter coral top (right side of image), which is attributed primarily to accelerating flow at the leading edge of the spherical bluff body. Normalized Reynolds stresses $\overline{u'w'}$ (Fig. 10b) exhibit a similar vertical profile compared to ADV measurements with low stresses

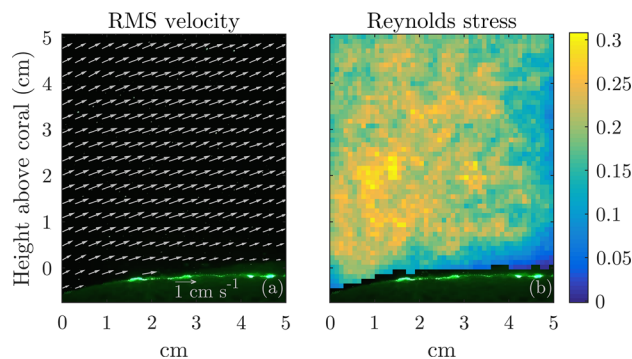
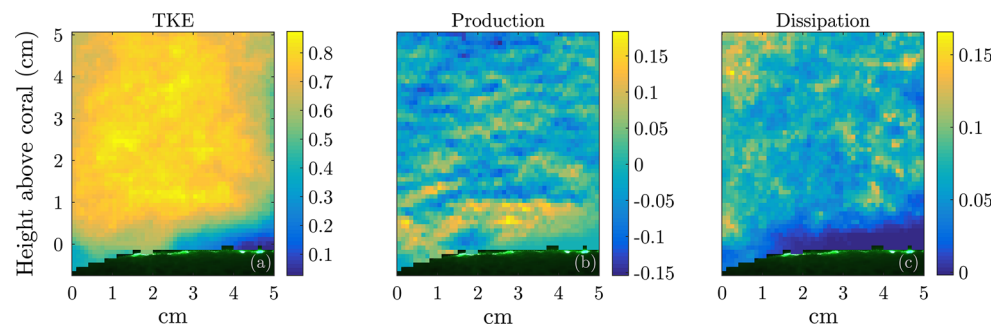


Fig. 10 a Vector field of normalized root-mean-square (rms) velocities over a healthy coral from particle image velocimetry. For clarity, only every third vector is plotted. **b** Plot of turbulent Reynolds stress $\overline{u'w'}$ normalized by square of rms free-stream velocity

Fig. 11 a Plot of turbulent kinetic energy over healthy coral normalized by square of root-mean-square (rms) free-stream velocity. Plots of turbulence production (b) and dissipation (c) normalized by cube of rms free-stream velocity



near the surface, a steep rise to peak values within 1 cm of the coral, and a gradual decrease for regions above $z = 2.5$ cm. The peak Reynolds stress values for the right half of the imaging window (~ 0.15 – 0.25) correspond well to ADV values, while the left half of the imaging window shows stress values nearly 50% higher and a much sharper gradient near the coral surface. The spatial variation in stresses agrees with similar spatial variations in velocity and suggests large-scale topography plays a significant role in creating spatial heterogeneity in the flow.

Normalized TKE (Fig. 11a) indicates a relatively constant value (~ 0.7 – 0.8) for elevations above 0.5 cm, which compares well to the TKE vertical profile seen in ADV measurements. Magnitudes of TKE, however, are higher for PIV data, likely owing to low particle seeding, which can create larger errors in instantaneous velocity estimates, thereby biasing terms in the TKE budget. Turbulence production (Fig. 11b) shows large peaks in the lowest 1 cm of the boundary layer and nearly zero production above this height, similar to the ADV profile, while turbulence dissipation (Fig. 11c) indicates low levels close to the surface and patchy increased rates higher in the water column. Peak normalized values for both production and dissipation are comparable to ADV estimates.

Discussion

Reef productivity and metabolism are driven both temporally and spatially by nutrient uptake rates, which have been shown to operate near the limits of mass transfer in reef communities (Falter et al. 2004). Under conditions of mass transfer limitation, nutrient uptake rates are physically limited by the transport of nutrients across concentration boundary layers, rather than biologically limited by rates of cellular transport and assimilation. This indicates that reef primary producers such as coral or algae take up nutrients as fast as physically possible, and thus, in the long term, flow-mediated enhancement of mass transfer can augment rates of benthic primary production. Predicting hydrodynamic control of nutrient mass transfer rates requires an adequate description of the near-bed turbulence

that is mechanistically correct at the scale of the inertial and concentration boundary layers (<1 mm). Our results indicate that two distinct fine-scale turbulent boundary layer regimes exist over healthy corals and algae-covered corals and that the transition from a wall-bounded inertial layer over healthy corals to a plane mixing layer regime over algae-covered corals has significant implications for mass transfer to corals.

Boundary layer characterization for healthy corals

Results describing mean and turbulence profiles over the healthy corals (Figs. 6, 8) suggest that key features of a canonical wall-bounded shear layer driven by combined wave-current flow are present. First, fully developed turbulent boundary layers possess an inertial sublayer defined by a logarithmic velocity profile (the “law of the wall”) extending $30 < z^+ < 300$, where $z^+ = u_*z/\nu$ is the dimensionless wall unit normalized by the viscous scale (Kundu and Cohen 2008). The agreement between the predicted and measured mean velocity profiles illustrated in Fig. 7 supports the existence of an inertial sublayer over the healthy corals. However, the plotted inertial subrange extends only to $z^+ \approx 60$, indicating transitional, rather than fully developed, turbulence (confirmed by the sub-critical wave Reynolds number). More energetic wave conditions—e.g., faster wave orbital velocities or larger wave orbital amplitudes—would enhance turbulence development, extending the sublayer vertical range and enhancing near-surface mixing.

A second feature of wall-bounded shear layers is the local balance of turbulence production and dissipation, evident in the TKE budget profiles in Fig. 8. Eddy production provides a main mechanism for advective fluid exchange between the coral surface and water column, driving scalar mixing and mass flux. To describe the length scale over which an overturning eddy mixes and the rate at which it advects, we estimated the turbulent mixing length ℓ_m and eddy viscosity ν_e , respectively, which scale linearly with distance from the wall according to $\ell_m = \kappa z$ and $\nu_e = u_*\kappa z$ (Kundu and Cohen 2008). Direct estimates of $\ell_m = |\overline{u'w'}|^{1/2}/|\partial u_{\text{rms}}/\partial z|$ and $\nu_e = -\overline{u'w'}/(\partial u_{\text{rms}}/\partial z)$ at

approximately 4 mm above the coral surface give mean values of $\ell_m = 0.16 \pm 0.1$ cm and $v_e = 0.64 \pm 0.4$ cm² s⁻¹, which closely match predicted values. Taken together, the agreement between experimental and predicted values for mean velocity, mixing length, and eddy viscosity, as well as the local balance in TKE components, strongly suggests that the turbulent boundary layer structure over the healthy corals is a canonical wall-bounded turbulent shear layer, and traditional log-layer dynamics can be used to parameterize predictions of flow and scalar flux.

Though ADV measurements taken on the flat section of the coral top suggest a wall-bounded shear layer, PIV results indicate that there is significant spatial heterogeneity in mean and turbulent flow dynamics across the varied topography of an individual coral. When describing the fine-scale boundary layer within centimeters of the coral surface, point measurements such as those recorded by an ADV may demonstrate only limited predictive value for considerations of integrated coral mass flux. Rather, estimates need to account for the effects of local topography and large-scale geometry on boundary layer dynamics, especially given that such variability influences coral morphological development and plasticity (Kaandorp et al. 1996).

Boundary layer characterization for algae-covered corals

Mean and turbulence profiles over algae-covered corals illustrate a much different boundary layer structure, more closely approximating a plane mixing layer. Similar to unconfined canopy flows in terrestrial systems, active turbulence at a canopy top forms when two co-flowing streams with different velocities interact along a midplane to produce a turbulent shear layer via propagation of Kelvin–Helmholtz instabilities (Nepf 2012). Several key hydrodynamic features characterize the plane mixing analogy for canopy turbulence. First, profiles of mean velocity and turbulent statistics exhibit strong vertical inhomogeneity, with a characteristic inflection point in velocity at the canopy top, and rapid decay of turbulent terms within the canopy—results evident in the rms velocity and TKE budget profiles. Qualitatively, the abrupt dampening of these terms within the canopy top is similar to many previously reported “dense” canopy flow profiles (Raupach et al. 1996).

The velocity inflection identifies the location of maximum shear and determines the canopy shear length scale according to $\ell_S = u_{\text{rms}}(h_c)/u'_{\text{rms}}(h_c)$, where h_c is the canopy height and the prime indicates a spatial derivative. ℓ_S controls the size of active turbulence above and within the canopy top (Raupach et al. 1996), and for the algae-covered corals, the mean shear length scale measures $\ell_S = 0.29 \pm 0.01$ cm, which compares well with reported values of 0.27–0.72 cm for a canopy of

equivalent height, where smaller values correlate with denser canopies (Finnigan 2000). Though this turbulent length scale is larger than the turbulent mixing length over the healthy coral, those eddies occur directly adjacent to the coral surface, whereas eddies induced by plane mixing occur at the canopy top and only have an overturning length $\sim 30\%$ of the canopy height. This indicates that momentum (and mass) is not actively exchanged with the lower parts of the canopy or the coral surface.

The plane mixing layer analogy for canopy flow suggests a significantly altered TKE budget profile, described by a local imbalance between production and dissipation in the “roughness sublayer”, i.e., the region just above the canopy ($h_c < z < 2h_c$) (Raupach et al. 1996). Production and dissipation profiles in Fig. 8 highlight this local imbalance, suggesting non-equilibrium turbulence in the roughness sublayer with significant pressure and turbulent transport vertically away from the coral surface. Finally, efficiency of momentum transfer can be measured by the Reynolds stress correlation coefficient, $r_{uw} = \overline{u'w'}/(\sigma_u\sigma_w)$, where σ_u and σ_w are standard deviations of horizontal and vertical velocity fluctuations, respectively. Typical values of r_{uw} for a plane mixing layer approach -0.5 , compared to -0.32 for an inertial layer, an indication of more effective momentum transfer (Raupach et al. 1996). Just above the canopy top, our results estimate $r_{uw} = -0.59 \pm 0.08$, matching predicted levels well and suggesting high momentum (and scalar) transfer in this region. Though the algal canopy enhances turbulent mixing and fluid exchange between the overlying water column and canopy top, its presence and density serve to buffer the coral surface from these exchanges and prevents the coral from benefitting from greater mixing rates.

Implications for biology

Many biological processes vital to coral health depend on the mean and turbulence flow structure near the coral surface, which control the diffusive boundary layer thickness and affect the mass flux “bottleneck”. Rates of mass flux m at the coral–water interface can be described by mass transfer theory according to $m = S(C_b - C_s)$, where C_b and C_s are the bulk fluid and surface nutrient concentrations, respectively, and S is a mass transfer coefficient dependent on molecular diffusivity and proportional to $\tau_{\text{bed}}^{1/2}$ (Hondzo 1998). This scaling suggests that for a fixed concentration gradient at the coral surface, the nearly nine times higher bed shear stress reported for healthy corals compared to algae-covered corals results in three times greater rates of mass transfer under the same ambient flow conditions. Though velocities reported here are relatively slow due to sheltering of the field site, faster flows should exhibit similar

effects as higher velocities would enhance bed shear stresses for both regimes; however, relative enhancements in mass flux would depend on the specific local conditions, such as surface roughness and canopy density.

Bed stress values alone, however, do not fully describe the hydrodynamic impact of the algal canopy. RMS velocity profiles between the two regimes, for example, demonstrate that the algal canopy dampens flow near the coral surface, which allows the DBL thickness to increase and reduces the efficacy of diffusive transport. Additionally, algal canopies actively photosynthesize, removing CO₂ before it reaches the coral surface (for use by zooxanthellae) and releasing O₂ adjacent to the surface, strengthening gradients in the DBLs of each species. More efficient mixing at the canopy top may produce a positive feedback loop, promoting algal primary productivity and growth while reducing a coral's physical access to nutrients.

Within a broader ecological context, these results may be important in the framework of shifting benthic community composition and a coral's ability to recover from large-scale natural or anthropogenic disturbances. Seasonal-scale events, such as hurricanes or disease outbreaks, and decadal-scale events, such as ocean warming and acidification, can physically damage reef structures and stress corals into bleaching events, rendering them vulnerable to invasion of algal competitors (Hoegh-Guldberg et al. 2007). Coral resilience depends on the ability to re-recruit expelled zooxanthellae, to efficiently exchange nutrients, and to mitigate thermal stress via advective transport. Turbulent hydrodynamics is a key driver of these processes. Our results demonstrate that the presence of an algal canopy on a coral surface shifts the turbulent boundary layer regime from a wall-bounded inertial layer to a plane mixing layer, and the hydrodynamic consequences of this transition lead to significant reductions in mass transfer, negatively impacting the ability of a coral to obtain resources and limiting its metabolic productivity.

Acknowledgments We thank Ross Timmerman, Alejandro Garcia-Chinchilla, Emma Hollowell, Mariam Trejos, and the Scientific staff at the Smithsonian Tropical Research Institute in Bocas del Toro, Panamá for field assistance.

Author contributions J. B. S., J. P. R., and M. A. R. conceived and designed the study, and collected the field data. J. B. S. performed the data and statistical analyses. J. B. S. and M. A. R. wrote the manuscript. All authors gave final approval for publication.

Funding This research was supported by the National Science Foundation (Grant NSF-OCE 1151314 to M. A. R.) and by the University of Virginia's Deepening Global Education grant program (to M. A. R.). Data are available through the data management plan implemented by the NSF-funded Long Term Ecological Research Station at the Virginia Coast Reserve at the website: <http://www.vcr.lter.virginia.edu>.

Compliance with ethical standards

Conflict of interest The authors declare no competing interests.

References

- Atkinson MJ, Bilger RW (1992) Effects of water velocity on phosphate uptake in coral reef-flat communities. *Limnol Oceanogr* 37:273–279
- Bendat JS, Piersol AG (2010) Random data: analysis and measurement procedures, 4th edn. Wiley, Hoboken
- Bricker JD, Monismith SG (2007) Spectral wave-turbulence decomposition. *J Atmos Ocean Technol* 24:1479–1487
- Brown A, Carpenter R (2013) Water-flow mediated oxygen dynamics within massive *Porites*–algal turf interactions. *Mar Ecol Prog Ser* 490:1–10
- Carpenter RC, Williams SL (1993) Effects of algal turf canopy height and microscale substratum topography of profiles of flow speed in a coral fore reef environment. *Limnol Oceanogr* 38:687–694
- Dennison WC, Barnes DJ (1988) Effect of water motion on coral photosynthesis and calcification. *J Exp Mar Bio Ecol* 115:67–77
- Falter JL, Atkinson MJ, Merrifield MA (2004) Mass-transfer limitation of nutrient uptake by a wave-dominated reef flat community. *Limnol Oceanogr* 49:1820–1831
- Falter JL, Atkinson MJ, Lowe RJ, Monismith SG, Koseff JR (2007) Effects of nonlocal turbulence on the mass transfer of dissolved species to reef corals. *Limnol Oceanogr* 52:274–285
- Finnigan J (2000) Turbulence in plant canopies. *Annu Rev Fluid Mech* 32:519–571
- Fredsøe J (1984) Turbulent boundary layer in wave-current motion. *J Hydraul Eng* 110:1103–1120
- Fricke A, Teichberg M, Beilfuss S, Bischof K (2011) Succession patterns in algal turf vegetation on a Caribbean coral reef. *Botanica Marina* 54:111–126
- Ghisalberti M, Nepf H (2006) The structure of the shear layer in flows over rigid and flexible canopies. *Environ Fluid Mech* 6:277–301
- Grant WD, Madsen OS (1979) Combined wave and current interaction with a rough bottom. *J Geophys Res* 84:1797–1808
- Gross TF, Nowell AR (1983) Mean flow and turbulence scaling in a tidal boundary layer. *Cont Shelf Res* 2:109–126
- Hoegh-Guldberg O, Mumby PJ, Hooten AJ, Steneck RS, Greenfield P, Gomez E, Harvell CD, Sale PF, Edwards AJ, Caldeira K, Knowlton N, Eakin CM, Iglesias-Prieto R, Muthiga N, Bradbury RH, Dubi A, Hatzios ME (2007) Coral reefs under rapid climate change and ocean acidification. *Science* 318:1737–1742
- Hondzo M (1998) Dissolved oxygen transfer at the sediment-water interface in a turbulent flow. *Water Resour Res* 34:3525–3533
- Jompa J, McCook LJ (2002) The effects of nutrients and herbivory on competition between a hard coral (*Porites cylindrica*) and a brown alga (*Lobophora variegata*). *Limnol Oceanogr* 47:527–534
- Jonsson IG (1966) Wave boundary layers and friction factors. *Coast Eng Proc* 10:127–148
- Jørgensen BB, Des Marais DJ (1990) The diffusive boundary layer of sediments: oxygen microgradients over a microbial mat. *Limnol Oceanogr* 35:1343–1355
- Kaandorp JA, Lowe C, Frenkel D, Sloat PMA (1996) The effect of nutrient diffusion and flow on coral morphology. *Phys Rev Lett* 77:2328–2331
- Kundu PK, Cohen IM (2008) Fluid mechanics. Academic, Burlington
- Li A, Reidenbach MA (2014) Forecasting decadal changes in sea surface temperatures and coral bleaching within a Caribbean coral reef. *Coral Reefs* 33:847–861

- Madsen OS, Poon Y-K, Graber HC (1988) Spectral wave attenuation by bottom friction: theory. *Coast Eng Proc* 21:492–504
- Mass T, Genin A, Shavit U, Grinstein M, Tchernov D (2010) Flow enhances photosynthesis in marine benthic autotrophs by increasing the efflux of oxygen from the organism to the water. *Proc Natl Acad Sci USA* 107:2527–2531
- McCook L, Jompa J, Diaz-Pulido G (2001) Competition between corals and algae on coral reefs: a review of evidence and mechanisms. *Coral Reefs* 19:400–417
- Monismith SG (2007) Hydrodynamics of coral reefs. *Annu Rev Fluid Mech* 39:37–55
- Nepf HM (2012) Flow and transport in regions with aquatic vegetation. *Annu Rev Fluid Mech* 44:123–142
- Nikora V, McEwan I, McLean S, Coleman S, Pokrajac D, Walters R (2007) Double-averaging concept for rough-bed open-channel and overland flows: theoretical background. *J Hydrol Eng* 133:873–883
- Raupach M, Finnigan J, Brunet Y (1996) Coherent eddies and turbulence in vegetation canopies: the mixing-layer analogy. *Bound Layer Meteorol* 60:375–395
- Reidenbach MA, Koseff JR, Monismith SG, Steinbuck JV, Genin A (2006a) The effects of waves and morphology on mass transfer within branched reef corals. *Limnol Oceanogr* 51:1134–1141
- Reidenbach MA, Monismith SG, Koseff JR, Yahel G, Genin A (2006b) Boundary layer turbulence and flow structure over a fringing coral reef. *Limnol Oceanogr* 51:1956–1968
- Reidenbach MA, Koseff JR, Monismith SG (2007) Laboratory experiments of fine-scale mixing and mass transport within a coral canopy. *Phys Fluids* 19:075107
- Reidenbach MA, George NT, Koehl MAR (2008) Antennule morphology and flicking kinematics facilitate odor sampling by the spiny lobster, *Panulirus argus*. *J Exp Biol* 211:2849–2858
- Røy H, Hüttel M, Jørgensen BB (2002) The role of small-scale sediment topography for oxygen flux across the diffusive boundary layer. *Limnol Oceanogr* 47:837–847
- Rusello PJ (2012) Near boundary measurements with a profiling acoustic Doppler velocimeter. *Hydraulic Measurement and Experimental Methods Conference*, August 12–15 2012, Snowbird, UT. American Society of Civil Engineers, Reston, VA, USA
- Shapiro OH, Fernandez VI, Garren M, Guasto JS, Debaillon-Vesque FP, Kramarsky-Winter E, Vardi A, Stocker R (2014) Vortical ciliary flows actively enhance mass transport in reef corals. *Proc Natl Acad Sci USA* 111:13391–13396
- Soulsby RL, Dyer KR (1981) The form of the near-bed velocity profile in a tidally accelerating flow. *J Geophys Res Oceans* 81:8067–8073
- Sveen JK (2004) An introduction to MatPIV v. 1.6.1. *Mechanics and applied mathematics*. Department of Mathematics, University of Oslo, Norway
- Voulgaris G, Trowbridge JH (1998) Evaluation of the acoustic Doppler velocimeter (ADV) for turbulence measurements. *J Atmos Ocean Tech* 15:272–289
- Wiberg P, Smith JD (1983) A comparison of field data and theoretical models for wave-current interactions at the bed on the continental shelf. *Cont Shelf Res* 2:147–162